NOAA ROSES Semi-Annual Report

Reporting Period: March 2021 – August 2021 (2nd report)

PI: Prof. Ping Yang (Texas A&M University)
Co-PI(s): Prof. Xianglei Huang (University of Michigan)

Project Title: Utilizing geostationary satellite observations to develop a next-generation ice cloud optical property model in support of JCSDA Community Radiative Transfer Model (CRTM) and JPSS CAL/VAL

Executive Summary (1 paragraph max)

This semi-annual report contains two parts: the first part summarizes of the research progress of the Texas A&M University team led by Prof. Ping Yang, and the second part summarizes of the research progress of the University of Michigan Co-I, Prof. Xianglei Huang.

Progress toward FY20 Milestones and Relevant Findings (with any Figs)

Texas A&M University accomplishments:

Task 1—Development of the next-generation ice optical property model

- Assessment of the assumptions used in the scattering property model development;
- Updates on the determination of the next-generation ice optical property model;
- Simulations of the single-scattering properties of various single hexagonal columns as part of the next-generation ice optical property model.

The surface roughness effect will be incorporated into the proposed next-generation ice optical property model. Due to inherent limitations in light scattering computational methods, some computational methods are not applicable to a roughness model. For example, ray-tracing based geometric optics methods use a conceptual surface roughness model, which cannot be incorporated into rigorous light scattering computational techniques (such as IITM; Bi et al., 2013). However, the development of a database of the single-scattering properties of ice crystals at a broad spectral range always requires multiple light scattering computational methods to compensate for limitations of specific methods for the single-scattering property computations. To begin the development of the database, the assessment of the various surface roughness models is essential. We first evaluate the consistency in the single-scattering properties among three surface roughness models including the conceptual roughness model, the geometrically roughened ice crystal model, and the randomly distorted ice crystal ensemble model. The three models are illustrated later in Figs. 1 and 2, with detailed description and explanation in the Fig. 1 caption.

The degree of surface roughness is defined as the variance (σ^2) of the two-dimensional (2D) Gaussian distributions (Yang and Liou, 1998), which describe the statistical distribution of the slope of a local planar facet of particles:

$$P(Z_x, Z_y) = \frac{1}{\pi\sigma^2} e^{-[(Z_x^2+Z_y^2)/\sigma^2]}, \quad (1)$$

where $Z_x = \partial Z/\partial x$ and $Z_y = \partial Z/\partial y$ are the slopes of a local particle surface facet along two direction orthogonal to the normal direction Z relative to the planar local particle surface.

The conceptual surface roughness incorporates the random tilting of rays of light at a surface facet of a particle through the ray tracing process in the light scattering computations (Fig. 1a). At each interaction between a ray of light and a particle surface, the local particle surface is tilted based on the following two angles:

$$\varphi_{\text{local}} = 2\pi\xi_1, \quad (2a)$$

$$\theta_{\text{local}} = \cos^{-1}[1/(1-\sigma^2 \ln \xi_2)], \quad (2b)$$

which obey the degree of surface roughness defined in Eq. (1), and ξ_1 and ξ_2 are two random numbers $(\xi_1, \xi_2) \in [0,1]$ that have uniform distributions. Hence, the slopes of a local particle surface are described as $Z_x = \partial Z/\partial x$ and $Z_y = \partial Z/\partial y$ in Eq. (1).

While conceptual surface roughness is an idealized model, the latter two surface roughness models explicitly consider the 3D particle geometry of a "roughened" particle surface. Geometric surface roughness considers microscopic surface texture explicitly in an ice crystal shape model (Fig. 1b). A particle face of a regular ice crystal is divided into a number of microscale facets, and each facet is randomly tilted based on the two angles equivalent to Eqs. (2) as described in Liu et al. (2013). Therefore, the random tilt of a microscopic facet of the particle surface obeys the degree of surface roughness in Eq. (1).

The surface roughness surrogate was introduced by Liu et al. (2014) using an ensemble of irregularly distorted ice crystals. Each facet of a regular ice crystal is tilted based on the two angles (φ_{macro} , θ_{macro}) equivalent to Eqs. (2), which alters a macroscopic shape of an ice crystal (referred to as an irregularly distorted ice crystal). A previous study implies quasi-equivalency in single-scattering properties between geometric surface roughness and an ensemble of a number of randomly distorted ice crystals (Liu et al., 2014).

As the random tilt process in these three roughness models obeys the same equations that are functions of the degree of surface roughness (hereinafter referred to using subscript "con", "geo", or "ens" for these roughness models, respectively), these three roughness models are mathematically comparable. The main difference among the three roughness models is the geometric scale of the surface roughness. The geometric surface roughness model is determined by σ^2_{geo} and the scale of a small facet. The ensemble surface roughness surrogate is determined by σ^2_{ens} and the number of randomly distorted ice crystals (N_{ens}) in the corresponding ensemble model.

Three state-of-the-science light scattering computational methods listed in Table 1 are used to compute the single-scattering properties of ice crystals with various roughness models. The invariant-imbedding T-matrix method (IITM) is applicable to arbitrarily shaped particles for accurate single-scattering property calculations based on electromagnetic theory (Bi et al., 2013). As the IITM does not rely on the geometric optics approximation, it does not use the conceptual roughness model for scattering property computations.

On the basis of the geometric optics principle, Yang and Liou (1996) developed an improved geometric optics method (IGOM) for efficient simulations of the single-scattering properties of arbitrarily shaped particles. Since IGOM incorporates the ray-spreading effect, the accuracy of the scattering property computations for intermediate sized particles is substantially improved as compared to the conventional geometric optics method. Furthermore, IGOM is applicable to all roughness models. An inherent limitation of IGOM is that the scattering property simulations at backscattering angles suffer from non-negligible uncertainty, as interference in

the scattering field associated with different rays is not taken into account.

The physical geometric optics method (PGOM; Yang and Liou, 1997) overcomes the IGOM limitation by implementing a rigorous near-field to far-field transformation and a finite sized beam instead of rays. As a result, PGOM achieves robust consistency in the simulation of the single-scattering properties of nonspherical particles, including the backscattering properties, with a rigorous IITM counterpart (Yang et al., 2019). The current PGOM is applicable only to convex particles, and therefore is not capable of simulating the single-scattering properties of ice crystals with explicit roughness texture.

Figures 1 and 2 show the phase matrix elements of the three roughened ice crystal models for a size parameter of 300, and degrees of surface roughness 0.03 (Fig. 1) and 0.15 (Fig. 2), respectively. Among a number of light scattering computational techniques, IGOM can simulate the single-scattering properties of the three roughness models. These two panels clearly indicate that these three roughness models are optically consistent each other.

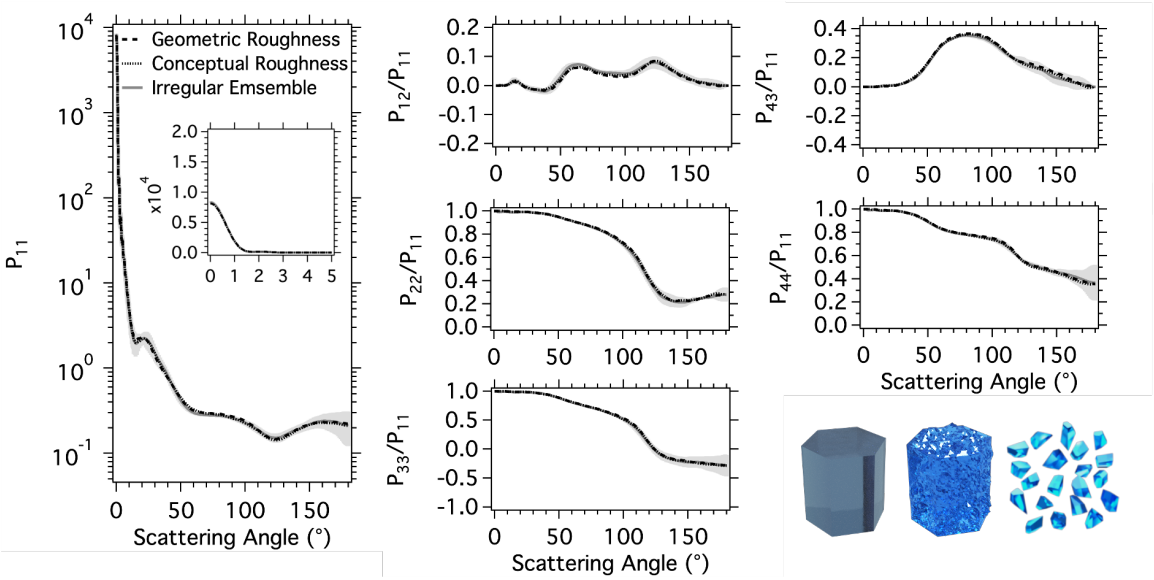

Figure 1. The six independent phase matrix elements of three roughened ice crystal models with a size parameter of 300 and a degree of surface roughness of 0.03. The shaded gray area is the envelope of phase matrix elements of the individual particles in the irregularly distorted ice crystal ensemble model, and the black solid line is the ensemble mean. The three roughened ice crystal models, illustrated at the lower right, are as follows: The conceptual roughness model is shown as a smooth hexagonal prism, but when each simulated ray encounters a surface, the surface normal is locally randomly tilted based on Eqs. (2a) and (2b). The geometric roughness model starts with the same hexagonal prism, but each face is covered with facets tilted in the same way by Eqs. (2). The irregularly distorted ice crystal ensemble model uses 20 hexahedra (not hexagonal columns), with each face of each hexahedron tilted in the same way as by Eqs. (2a) and (2b).

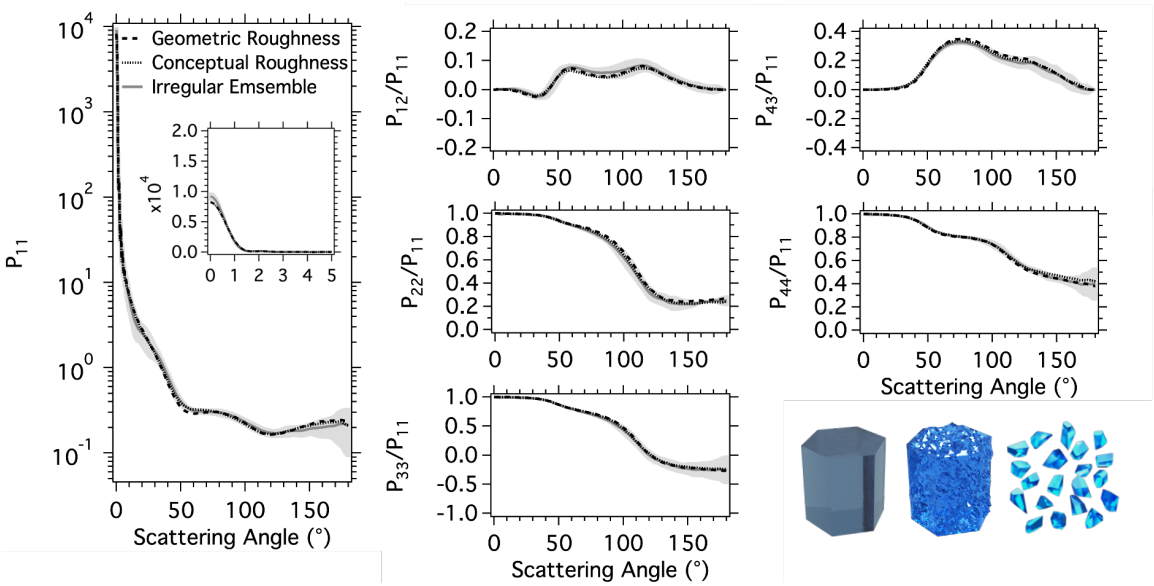

Figure 2. Same as Fig. 1 but with degree of surface roughness 0.15.

Figure 3 shows the extinction efficiency as a function of the size parameter, indicating robust consistency among the three roughness models. This confirms the effective equivalency in the single-scattering properties of these roughened ice crystal models under the geometric optics principle. In the development of the next-generation ice optical property model, we will use geometrically roughened ice crystal shapes for IITM computations, and an idealized roughness model for IGOM computations.

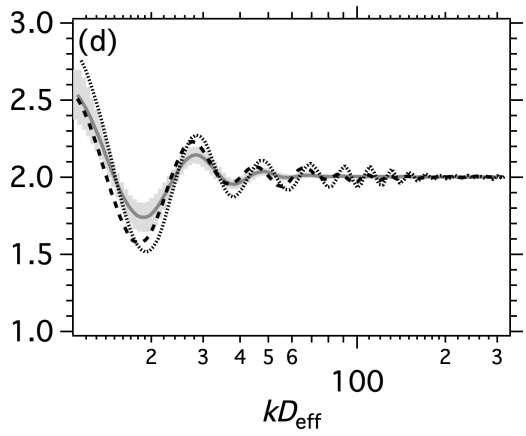

Figure 3. Extinction efficiencies of three roughened ice crystal models (shaded gray area and lines have the same meanings as in Fig. 1) as a function of the size parameter in the horizontal axis with the degree of surface roughness 0.5.

Figure 4 illustrates the particle shape models for the next-generation ice optical property model. Compared to the proposed particle shape model reported in the last project report, we have added an additional particle model, consisting of 20 particles, each of which is an aggregate of irregular hexagonal columns. For single hexagonal columns, we consider 9 different aspect ratios ranging from 0.1 (i.e., hexagonal plates) to 10 (i.e., hexagonal columns), and 7 degrees of surface roughness from 0 to 0.5.

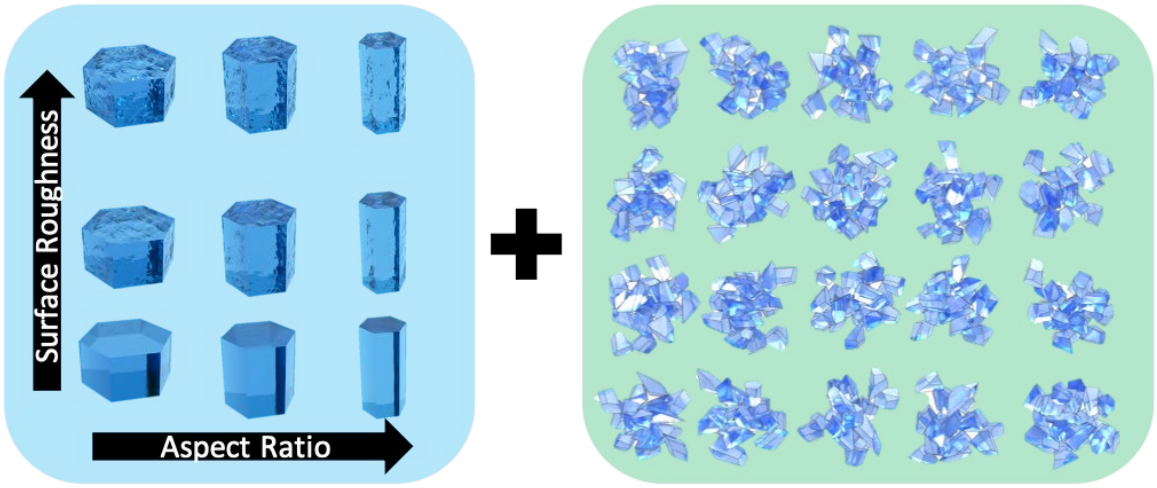

Figure 4. Ice crystal shape models to be used for the next-generation ice optical property model. This is called the two-habit model (THM), and as the average particle size in an ice cloud increases, the proportion of single hexagonal columns decrease, and aggregate particles increase.

1.2.1.3. Simulations of the single-scattering properties of various single hexagonal columns as part of the next generation ice optical property model

As the proposed model incorporates temperature dependence of the ice refractive index, we apply the kernel technique (Saito et al., 2021) to organize the database and split the relevant spectrum into 6 spectral domains (wavelength boundaries listed in Table 1; abbreviations are ultraviolet-visible [UV-VIS], near infrared [NIR], shortwave IR [SWIR], thermal IR [TIR]) as illustrated by different color rectangles in the right panel of Fig. 5. The scattering property kernels are organized according to size parameter instead of a combination of the wavelength and size, which compresses the total data size of the database and reduces the required total computational resources for the database development.

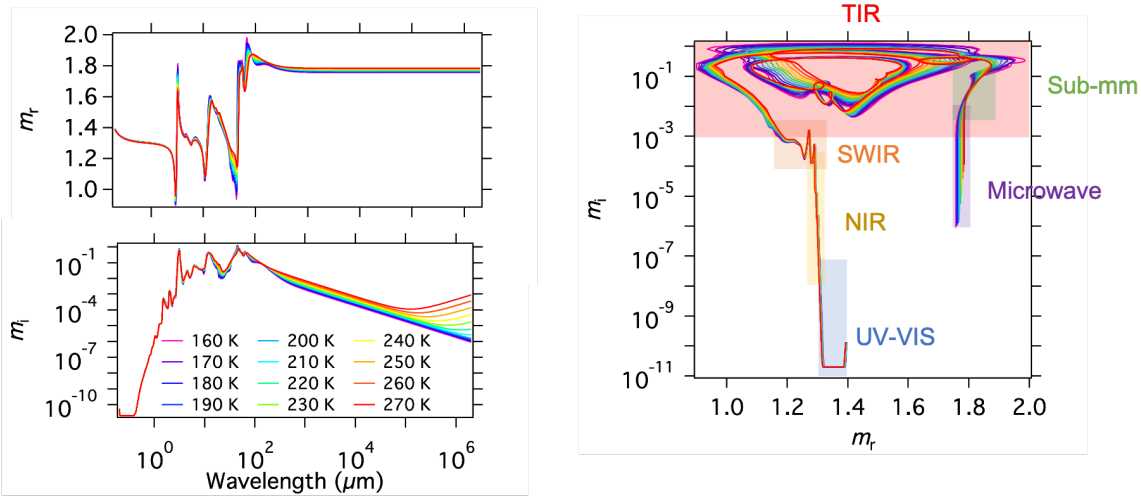

Figure 5. The real part (m_r) and imaginary part (m_i) of the ice refractive index from UV to microwave domains. Table 1 lists wavelength boundaries of the six domains.

Table 1 describes the configurations (wavelength, size parameter, and refractive index) of the single-scattering database. Effects of surface roughness are considered in UV-VIS, NIR, and SWIR domains but ignored in other domains as the particle surface roughness has little impact.

Table 1. General configuration of the database (l = wavelength, x = size parameter, N_x = number of size parameter values in database, m_r = real part of refractive index, m_i = imaginary part of refractive index).

	UV-VIS	NIR	SWIR	TIR	Sub-mm	Microwave
l_{min}	0.17 μm	0.95 μm	1.45 μm	2.7 μm	85 μm	1000 μm
l_{max}	0.95 μm	1.45 μm	2.7 μm	85 μm	1000 μm	20000 μm
x_{min}	10	6.81292	3.16228	0.1	<0.01	<0.01
x_{max}	383119	100000	68129.2	31622.8	1000	100
N_x	74	71	77	91	85	67
m_{r_min}	1.298538	1.281838	1.141254	0.9	1.749894	1.749894
m_{r_max}	1.398107	1.316228	1.316228	2.0	1.891251	1.794328
N_m_r	6	3	8	29	4	2
m_{i_min}	1.0e-11	3.16228e-7	1.0e-4	1.0e-3	1.33352e-3	1.0e-6
m_{i_max}	1.0e-6	3.16228e-4	3.16228e-3	1.77828	3.16228e-1	1.0e-2
N_m_i	4	13	13	14	20	33

The size parameter bins have a constant logarithmic interval except for twice the resolution in a size parameter range between 3.16228 and 316.228, as the scattering properties in that size parameter domain show moderately nonlinear dependence. We apply IITM computations for size parameters less than 50–100, and IGOM for larger particles. Table 2 summarizes the current progress of the scattering property computations for the database development as of July 31st 2021. Note that the scattering property computations require substantial computational resources.

Table 2. The current progress of the scattering property computations for the next-generation ice optical property model development.

	UV-VIS	NIR	SWIR	TIR	Sub-mm	Microwave
IITM (smooth)	100%	100%	90%	75%	100%	100%
IITM (rough)	20%	5%	0%	N/A	N/A	N/A
IITM (aggregate)	0%	0%	0%	0%	0%	0%
IGOM (smooth)	100%	100%	100%	100%	100%	N/A
IGOM (rough)	100%	100%	100%	N/A	N/A	N/A
IGOM (aggregate)	0%	0%	0%	0%	0%	N/A

Task 2—Procedures and dataset for the consistency evaluations of the next-generation ice optical property model

- Create fused dataset that collocates atmospheric profiles, radiative signals, and surface characteristics in the same pixel;
- Improve the data sampling techniques of the GOES-16/17 radiative signals to minimize retrieval biases.

For the purpose of conducting the retrievals, it is necessary to collocate all required data in the same pixel, including atmospheric profiles, radiative signals, and surface characteristics. We express all data in 2-km GOES-16 resolution, because most GOES-16 products are in 2-km resolution, and the computational efficiency would be improved by using relatively coarse spatial resolution. Table 3 below summarizes the products whose spatial resolution needs to be converted. Linear interpolation is applied to convert products with coarser spatial resolution into 2-km resolution. For the products with higher spatial resolution, such as GOES-16 reflectance

data in band 2 and band 3, two downscaling methods can effectively solve this problem, which will be explained in 2.2.2.

Table 3. Summary of the converted products

Products	Spatial Resolution
GOES-16 Cloud Top Pressure (CTP)	10×10 km
GOES-16 Cloud Top Height (CTH)	10×10 km
GOES-16 Land Surface Temperature (LST)	10×10 km
GOES-16 Cloud Optical Depth (COD)	4×4 km
GOES-16 Reflectance at band 2 (REFC2)	0.5×0.5 km
GOES-16 Reflectance at band 3 (REFC3)	1×1 km
MCD43C3 White Sky Albedo (WSA)	0.05×0.05 degree
MOD11 Monthly Land Surface Temperature (MLST)	0.05×0.05 degree
MERRA-2	50×50 km

Figure 6 shows the interpolation result of GOES-16 CTP, CTH, LST products, and MERRA-2 ozone mixing ratio data at 850 hPa, 550 hPa and 250 hPa level in 2-km resolution at 18:00 pm (UTC) on August 25, 2017. The GOES-16 LST data presented here are combined with MOD11 monthly land surface temperature data, since there are many invalid values in GOES-16 LST data. The MERRA-2 data contains 8 dimensions of time, 42 levels and 14 variables, including ozone mass mixing ratio, surface geopotential height, and air temperature. We use ozone mass mixing ratio data as an example to show its distribution at three different levels after linear interpolation. These converted products in 2-km resolution all show good consistency with their original product.

Since the spatial resolution of GOES-16 reflectance data is 0.5 km in band 2 and 1 km in band 3, two methods for pixel downscaling introduced in GOES-R ABI ATBD for cloud and moisture imagery products are used in this study. Method 1 is to regularly omit several pixels to downscale the data, which is called subsampling, and Method 2 is to average surrounding pixels to convert 0.5-1 km into 2-km data (Schmit et al., 2010). Although the first method is faster and more straightforward than the second one, this could lead to systematic biases depending on horizontal scales of clouds, which could significantly affect the retrieval results. For instance, a spatial scale of some clouds might be as small as a 0.5-1 km pixel, and their contribution could be simply omitted by using the first method. Therefore, we evaluate impacts of these downscaling techniques on GOES-16 bands 2 and 3 reflectance data for various cloud types classified based on the International Satellite Cloud Climatology Project (ISCCP) cloud classification diagram.

Figure 7 shows the comparison results of GOES-16 band 2 and band 3 reflectance data between these two methods for different types of high clouds (cloud top pressure range from 0 – 440 hPa) in ocean regions based on the ISCCP cloud classification diagram. Cirrus cloud has the smallest correlation coefficient in both band 2 and band 3 reflectance data due to its small spatial scale. For other high clouds, such as Cirrostratus and Cumulonimbus, there are also some discrepancies between these downscaling methods. The consistency of these two methods for reflectance in band 3 is even worse than in band 2. It is widely known that the reflectance data is essential for the Nakajima-King retrieval. Inconsistency between these two methods can cause significant biases to the retrieved ice optical property, then can affect the identification of the optimal ice cloud model, which would eventually hinder the development of the next-generation ice optical property model. Therefore, an objective of this project is to investigate the impacts of these downscaling methods on the ice cloud property retrievals for different types of high clouds.

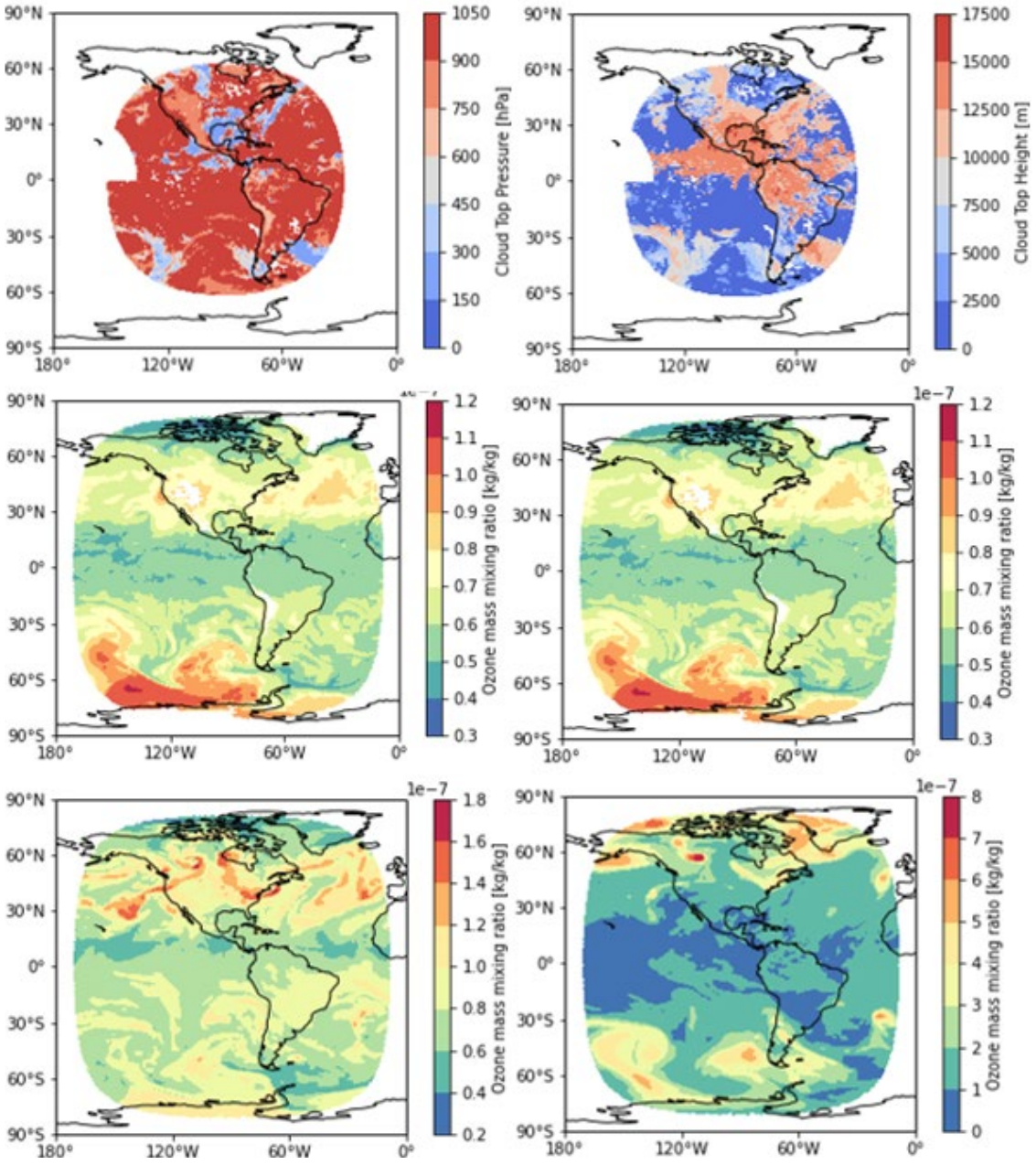

Figure 6. The converted GOES-16 CTP, CTH, and LST products (first column) and MERRA-2 ozone mass mixing ratio at 850 hPa, 550 hPa and 250 hPa level (second column) in 2-km resolution at 1800 (UTC) on August 25, 2017.

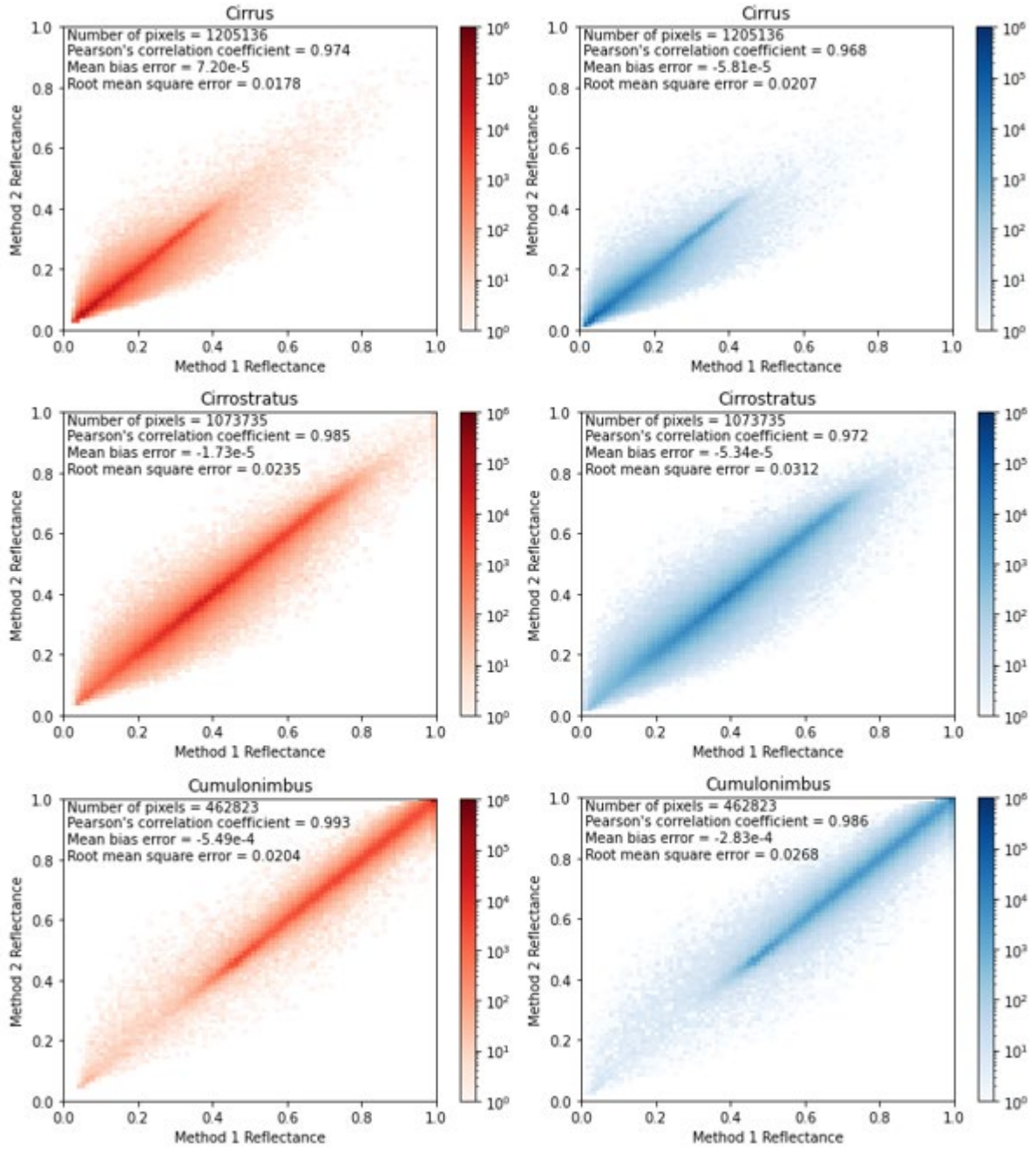

Figure 7. Comparison of the converted GOES-16 band 2 (left column) and band 3 (right column) reflectance data at 1800 (UTC) on August 25th, 2017, between two downscaling methods for different types of clouds in ocean regions based on the ISCCP cloud classification diagram.

University of Michigan accomplishments:

In the first half year, the University of Michigan (UM) team has assessed the clear-sky radiative transfer calculation of CRTM2.4.0 with benchmark line-by-line radiative transfer model (LBLRTM12.0; Clough et al., 2005) and another widely used radiative transfer model in Earth remote sensing community, Moderate Transmission Code version 5 (MODTRAN5; Anderson et al., 2007), which has been reported in the previous progress report. In the second half year, we have continued this line of work and carried out further assessment for cloudy-sky radiative transfer calculations using CRTM2.4.0 and MODTRAN5. The default tropical profile in CRTM

2.4.0 is used. Cloud is assumed to be overcast and between 400-500 hPa, i.e., all ice clouds and no liquid clouds. The effective radius of ice particle is set at 20 μm. The spectrally varying optical properties of ice clouds are based on a publication by the PI's group, i.e., Kuo et al. (2020), for both CRTM 2.4.0 and MODTRAN5 calculations. The MODTRAN5 calculates radiances at a higher spectral resolution and the results are convolved with GOES-16 and GOES1-7 ABI spectral response functions, respectively. Note CRTM 2.4.0 employed an adding-doubling scheme to solve the multiple scattering radiative transfer, while we used 8-stream DISORT solver in MODTRAN5 for multiple scattering calculation.

The results and comparisons between CRTM2.4.0 and MODTRAN5 are shown in Fig. 8. For small ice water path (IWP = 6 g m^{-2}, visible optical depth ~0.46), the simulated bright temperature at each ABI channels by MODTARN5 and CRTM 2.4.0 (black lines in the left panels) agree well with each other. The large difference is well within ±3K in brightness temperature. Such agreement is consistent with the favorable comparisons of clear-sky calculation shown in the previous report. For large ice water path, IWP = 30 g m^{-2} (visible optical depth ~2.3), the difference between CRTM 2.4.0 and MODTRAN5 becomes much larger. The difference, in brightness temperature, is as large as -10.5K for the 8.4-μm channel and -7K for the 12.3-μm channel. For this large IWP case, CRTM2.4.0 simulated radiance is smaller than MODTRAN5 counterpart for all mid-IR window channels.

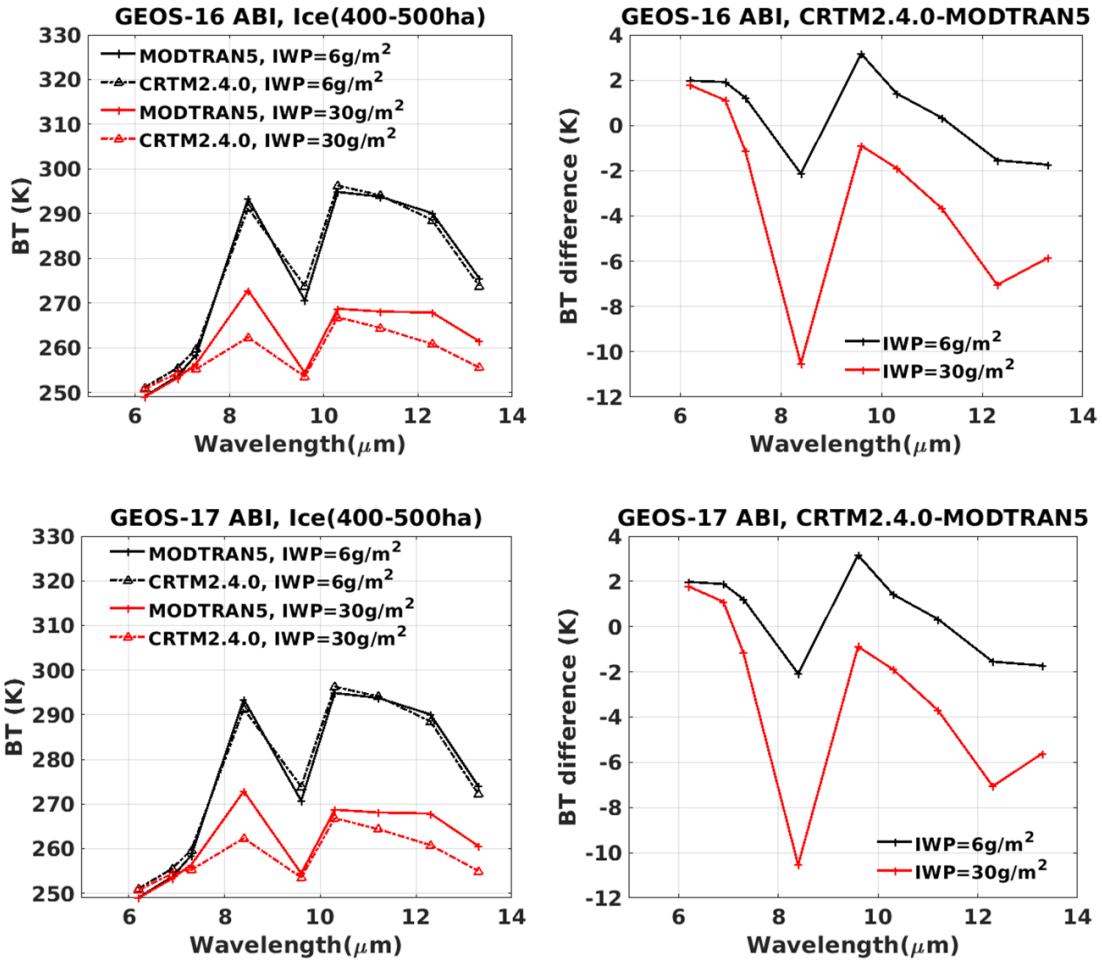

Figure 8. Upper right panel: the simulated brightness temperatures at GEOS-16 ABI infrared channels for overcast ice cloud at 400-500 hPa with different ice water paths (IWPs). The

meaning of each curve is shown in the legend. Upper left panel: the difference between CRTM2.4.0 and MODTRAN5 calculation for two IWPs as labeled. Lower panels: same as the upper panels except for GEOS-17 ABI.

We have also discovered that the built-in test cases in the CRTM 2.4.0 have issues in its default temperature profiles. For example, the built-in tropical profile in the CRTM 2.4.0 has a surface temperature as high as 315.2K (which should be ~299K); and the built-in US standard profile has a surface temperature only 273K (which should be 288K). While these profiles can be still used in radiative transfer calculation, they are not representative for the respective scenarios.

Plans for Next Reporting Period

In the next 6 months, the TAMU team will continue the single-scattering property computations to develop the next-generation ice optical property model. In addition, we will improve the retrieval system for the consistency check ice cloud property retrievals using GOES-16/17 and CALIOP observations. Furthermore, we will evaluate CRTM after the next-generation ice optical property model is incorporated into CRTM, which will be scheduled around the end of Year 2 or the beginning of Year 3. The U Michigan team will continue the comparison to understand why MODTRAN5 and CRTM 2.4.0 differ so much in terms of the simulation over the ABI IR window channels. Our premise is that it is the treatments of multiple scattering that leads to such big difference, as the difference is shown to vary with cloud optical depth and the difference is much less over the H_2O channels (i.e., 6.2 and 6.9 μm). The treatment of water vapor foreign continuum absorption can also contribute to such difference, which we will also investigate upon. These will help us further understand and assess the infrared radiative transfer solver in the CRTM 2.4.0 in the presence of clouds.

References:

Anderson, G. P., A. Berk, J. H. Chetwynd, J. Harder, J.M. Fontenla, E.P. Shettle, et al., 2007: Using the MODTRAN™5 radiative transfer algorithm with NASA satellite data: AIRS and SORCE. Proc. SPIE, 6565, 65651O. http://dx.doi.org/10.1117/12.721184.

Bi, L. P. Yang, G. W. Kattawar, and M. I. Mishchenko, 2013: Efficient implementation of the invariant imbedding T-matrix method and the separation of variables method applied to large nonspherical inhomogeneous particles, *J. Quant. Spectrosc. Radiat. Transfer,* **116**, 169–183.

Clough, S. A., M. W. Shephard, E. J. Mlawer, J. S. Delamere, M. J. Iacono, K. Cady-Pereira, S. Boukabara, and P. D. Brown, 2005: Atmospheric radiative transfer modeling: A summary of the AER codes, J. Quant. Spectrosc. Radiat. Transfer, 91, 233–244, https://doi.org/10.1016/j.qsrt2004.05.058.

Kuo, C.-P., P. Yang, X. L. Huang, Y.-H. Chen, G.S. Liu, 2020: Assessing the accuracy and efficiency of longwave radiative transfer models involving scattering effect with cloud optical property parameterizations, Journal of Quantitative Spectroscopy and Radiative Transfer, 240, 106683, 10.1016/j.jqsrt.2019.106683.

Liu, C., Panetta, R. L., and Yang, P. 2013: The effects of surface roughness on the scattering properties of hexagonal columns with sizes from the Rayleigh to the geometric optics regimes, *J. Quant. Spectrosc. Radiat. Transf.,* **129,** 169-185.

Liu, C., Panetta, R. L., and Yang, P. 2014: The effective equivalence of geometric irregularity and surface roughness in determining particle single-scattering properties, *Opt. Express,* **22,** 23620-23627.

Saito, M., Yang, P., Ding, J., & Liu, X., 2021: A comprehensive database of the optical properties of irregular aerosol particles for radiative transfer simulations. *Journal of the Atmospheric Sciences*, in press, https://doi.org/10.1175/JAS-D-20-0338.1

Schmit, T. J., Gunshor, M. M., Fu, G., Rink, T., Bah, K., & Wolf, W., 2010: GOES-R Advanced Baseline Imager (ABI) Algorithm Theoretical Basis Document for Cloud and Moisture Imagery Product. Version 2.3. *Noaa Nesdis Star*, 62.

Yang, P., and K. N. Liou, 1996: Geometric-optics-integral-equation method for light scattering by nonspherical ice crystals, *Appl. Opt.*, **35,** 6568–6584.

Yang, P., and K. N. Liou, 1997: Light scattering by hexagonal ice crystals: Solution by a ray-by-ray integration algorithm, *J. Opt. Soc. Amer. A.*, **14,** 2278-2289.

Yang, P. and K. N. Liou, 1998: Single-scattering properties of complex ice crystals in terrestrial atmosphere, *Contr. Atmos. Phys.*, **71 (2),** 223–248.

Yang, P., Ding, J., Panetta, R. L., Liou, K.-N., Kattawar, G. W., & Mishchenko, M. I., 2019: On the convergence of numerical computations for both exact and approximate solutions for electromagnetic scattering by nonspherical dielectric particles, *Progress in Electromagnetic Research*, 164, 27–61.